


Design optimization of an automobile torque arm using global and successive surrogate modeling approaches

Proc IMechE Part D:
J Automobile Engineering
2019, Vol. 233(6) 1453–1465
© IMechE 2018
Article reuse guidelines:
sagepub.com/journals-permissions
DOI: 10.1177/0954407018772739
journals.sagepub.com/home/pid


Erdem Acar, Nahide Tüten and Mehmet Ali Güler

Abstract

The design of lightweight automotive structures has become a prevalent practice in the automotive industry. This study focuses on design optimization of an automobile torque arm subjected to cyclic loading. Starting from an available initial design, the shape of the torque arm is optimized for minimum weight such that the fatigue life of the torque arm does not fall below that of the initial design and the maximum von Mises stress developed in the torque arm does not exceed that of the initial design. The stresses are computed using ANSYS finite element software, and the fatigue life is calculated using the Smith–Watson–Topper model. Surrogate-based optimization approach is used to reduce the computational cost. Optimization results based on global surrogate modeling and successive surrogate modeling approaches are compared. It is found that the successive surrogate modeling approach results in 28.7% weight reduction for the torque arm, whereas the global surrogate modeling approach results in 25.7% weight saving for the torque arm.

Keywords

Fatigue, finite element analysis, optimization, surrogate model, global surrogate modeling, successive surrogate modeling

Date received: 12 June 2017; accepted: 23 March 2018

Introduction

Structural performance evaluation of automobile structures is usually performed through finite element analyses. Venkataraman and Haftka¹ noted that despite the remarkable growth of computer processing power, capacity, and storage, the finite element models with acceptable accuracy still require substantial central processing unit (CPU) time. For instance, Fang et al.² noted that it takes about 15–20 h of CPU time to run one automobile crash simulation, even with a high level of computational power. Therefore, the optimization studies that require repeated analyses become computationally intractable. To alleviate the computational cost of optimization, surrogate models that can approximate the results of simulation models can be used. This approach is often called the surrogate-based optimization.

The most popular surrogate modeling techniques in practice include polynomial response surface approximations,^{3,4} kriging,^{5,6} radial basis functions,^{7,8} neural networks,^{9,10} and support vector regression.^{11,12} As it is difficult to know a priori the most accurate surrogate model and as it is important to safeguard against choosing a wrong surrogate model, combined use of multiple

surrogate models in the form of an ensemble has also been pursued.^{13–15}

Surrogate-based optimization strategies are twofold: (1) a global surrogate model is constructed (for each response of interest) over the entire design space, and (2) a series of local surrogate models is constructed. When a global surrogate model is used, first a sufficiently accurate surrogate model is generated, which is then used to perform optimization in a single step. This strategy is often used in surrogate-based optimization studies.^{16,17} On the contrary, when a series of local surrogate models is used, optimization is performed in an iterative (multi-step) procedure, and local surrogate models are generated around the optimum found in the previous step. An example of this strategy is the successive response surface method used in Roux et al.¹⁸ and Stander and Craig.¹⁹

Department of Mechanical Engineering, TOBB University of Economics and Technology, Ankara, Turkey

Corresponding author:

Erdem Acar, Department of Mechanical Engineering, TOBB University of Economics and Technology, Söğütözü, Ankara 06560, Turkey.
Email: acar@etu.edu.tr

Surrogate-based optimization of automobile structures has been investigated by many researchers. Most of these studies are based on the use of global surrogate models. Sobieszczanski-Sobieski et al.²⁰ used global response surface approximations in design optimization of a car body structure for minimum weight under the constraints of noise, vibration, harshness, and a crash event. Youn et al.²¹ used global response surface models generated using stepwise regression to perform reliability-based design optimization of an automobile subject to a side impact. Zhang et al.²² used global response surface models to conduct robust lightweight design optimization of an automotive front side rail. Lee and Kang²³ used global kriging models to perform structural optimization of an automotive door. Kim et al.²⁴ used global kriging models to perform structural design optimization of an outer tie rod of a passenger car. Liu et al.²⁵ used global kriging models to perform lightweight design of an automotive composite bumper system. Kiani et al.²⁶ used global radial basis function surrogate models to optimize automotive structures under multiple crash and vibration design criteria. Hu et al.²⁷ used global radial basis function surrogate models to optimize the aerodynamic shape parameters of an automobile to minimize aerodynamic drag and aerodynamic lift. Yildiz et al.²⁸ as well as Karagöz and Yildiz²⁹ used global radial basis functions in structural design optimization of automotive components to minimize weight and maximize energy absorption, respectively. Zhu et al.³⁰ used support vector regression surrogate models to optimize the roof crush resistance force and to obtain lightweight design of vehicle front end structure subject to frontal crash event. Fan et al.³¹ used global support vector regression surrogate models to perform shape optimization of a green technology automobile. Song et al.³² used artificial neural networks to conduct aerodynamic design optimization of rear body shapes of a sedan automobile to minimize the drag. Zhu et al.³³ used back-propagation neural networks to design a new automotive door sealing.

In addition to the surrogate-based optimization of automobile structures based on the use of global surrogate models, there also exist studies based on the use of a series of local surrogate models (successive surrogate modeling, SSM). Kurtaran et al.³⁴ used the SSM approach to optimize a simplified vehicle crashing into a rigid pole and optimized the New Jersey concrete barrier. Craig et al.³⁵ used SSM to optimize an automotive structure under frontal impact. Thiele et al.³⁶ used SSM to optimize an adaptive restraint system. Liang and Le³⁷ used SSM to optimize the energy absorption ability of bus frame components. The SSM approach has also been used in design optimization studies other than automotive structural design. Gustafsson and Strömberg³⁸ used SSM to perform shape optimization of castings. Zhang et al.³⁹ used SSM for identification of material parameters of high-strength steel under impact loading. Pajunen and Heinonen⁴⁰ used SSM to perform design optimization of marine structures. The

common finding of these studies is that the SSM approach converges at reasonable number of iterations (e.g. eight iterations in Craig et al.³⁵ and seven iterations in Liang and Le³⁷); hence, SSM is a competitive alternative to the global surrogate modeling approach. Inspired from these findings, global surrogate modeling and SSM approaches are used, and their results are compared in this study.

The objective of this paper is to perform design optimization of an automobile torque arm subjected to cyclic loading using SSM. The rest of the paper is organized as follows. The definition of the optimization of the torque arm for minimum weight is presented in section "Problem definition." Section "Fatigue tests" provides details of the fatigue life estimation of the torque arm by the use of finite element analysis. Global surrogate modeling and SSM strategies followed in this study are detailed in section "Finite element modeling." The results and the concluding remarks are given in sections "Successive surrogate modeling" and "Results," respectively.

Problem definition

In this study, weight optimization of an automobile torque arm subjected to cyclic loading is conducted. The torque arm is a component of an automobile suspension system mounted on the rear-drive axle and allows the automobile to accelerate in a straight line without rotation of the rear axle. The torque arm design optimization problem considered in this study was first studied by Botkin⁴¹ and then used in many optimization studies, including Wang et al.,⁴² Kim et al.,⁴³ and Picheny et al.⁴⁴ Botkin⁴¹ and Wang et al.⁴² performed shape optimization of the torque arm under static loading by using stress as well as displacement constraints. Kim et al.⁴³ and Picheny et al.⁴⁴ conducted similar studies but used stress constraint only. Instead of static loading, this paper takes cyclic loading on the torque arm into account (which is more representative of the actual loading conditions), along with the static failure criteria, and performs shape optimization of the torque arm under fatigue life and stress constraints. Note that the use of fatigue life in design optimization of automotive parts is considered in many studies, including Karen et al.⁴⁵ and Yildiz and Lekesiz.⁴⁶

The initial geometry of the torque arm, along with the loading and boundary conditions corresponding to the actual working conditions, is shown in Figure 1. The torque arm is fixed to the chassis at the left end, and the cyclic loads F_X and F_Y transferred from the rear wheels are applied at the right end. The nominal values of F_X and F_Y used are 695.25 and 1266.50 N based on earlier studies.^{43,44} The cyclic loads F_X and F_Y are assumed to vary between -0.79 and 1.10 times of their corresponding nominal values (i.e. the stress ratio is -0.718), according to the multi-axial fatigue loading standard for car wheel suspensions, CARLOS-multi.⁴⁷

Table 1. Properties of the torque arm material (AISI 1040 carbon steel).

Property	Value
Young's modulus (E)	201.6 GPa
Poisson's ratio (ν)	0.26
Bulk modulus (κ)	140 GPa
Yield strength (σ_Y)	415 MPa
Ultimate strength (σ_U)	620 MPa
Fatigue strength coefficient (σ'_f)	1543 MPa
Fatigue strength exponent (b)	-0.14
Fatigue ductility coefficient (ϵ'_f)	0.61
Fatigue ductility exponent (c)	-0.57

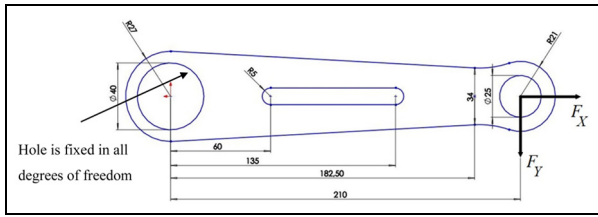


Figure 1. Loading and boundary conditions on the torque arm corresponding to the actual working conditions (dimensions in mm).

The thickness of the torque arm is 3 mm, and it is made of AISI 1040 carbon steel, the properties of which are given in Table 1.

As noted earlier, according to the actual working conditions, the torque arm is fixed to the chassis at the left end; hence, fixed-end boundary conditions are used. However, in our fatigue tests (see section “Fatigue tests”), we could not satisfy the fixed-end boundary conditions. Therefore, we first generated a finite element model with boundary conditions similar to the test conditions and then compared the FE model fatigue life prediction with the fatigue life observed in the tests. This allowed us to make sure that the correct fatigue failure criterion was used, three-dimensional (3D) analysis rather than two-dimensional (2D) analysis was required, and proper finite element meshing is applied. After this step, we changed the boundary conditions at the left end and performed optimization using the revised finite element model.

Figure 2 shows the five geometric properties (d_1 , d_2 , h_1 , h_2 , and v_1) used as design variables in optimization. The variables d_1 and d_2 are the diameters at the left and right of the slit in the torque arm, h_1 and h_2 are the horizontal distances of the centers of the left and right circles of the slit, and v_1 is the shape variable that defines the outer shape of the torque arm. Earlier studies^{41–44} have confirmed that the selection of these design variables leads to substantial weight savings from the torque arm without jeopardizing the safety. Therefore, these particular geometric properties and the design variables are also used in this study.

The objective function of the optimization problem is the mass of the torque arm. The fatigue life and the

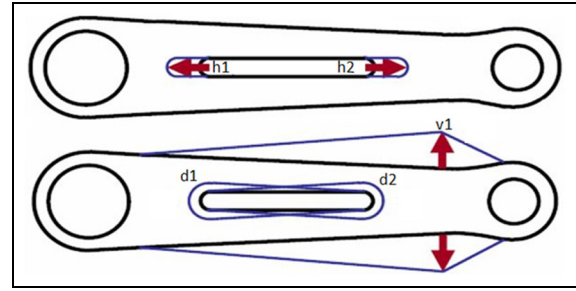


Figure 2. Design variables of the torque arm.

maximum von Mises stress developed in the torque arm are constrained to the corresponding values of the initial design. Thus, the static and the fatigue performances of the torque arm are taken into account. The optimization problem can be formulated as follows

$$\begin{aligned}
 & \text{Find } d_1, d_2, h_1, h_2, v_1 \\
 & \text{Min } m(d_1, d_2, h_1, h_2, v_1) \\
 & \text{S.t. } \sigma_{VM}(d_1, d_2, h_1, h_2, v_1) \leq (\sigma_{VM})_{ini} \\
 & \quad N_f(d_1, d_2, h_1, h_2, v_1) \geq (N_f)_{ini}
 \end{aligned} \tag{1}$$

where $m()$ represents the mass, $\sigma_{VM}()$ represents the maximum von Mises stress developed in the torque arm, $(\sigma_{VM})_{ini}$ is the maximum von Mises stress corresponding to the initial design, $N_f()$ represents the fatigue life (number of cycles) of the torque arm, and $(N_f)_{ini}$ is the fatigue life of the initial design. The maximum von Mises stress and fatigue life are computed through finite element analyses.

Fatigue tests

To provide a baseline for comparison of the fatigue lives computed by finite element analyses, fatigue tests are conducted at the Technology Center of the TOBB University of Economics and Technology. Labiotech HH300K-OC fatigue test machine with the following features is used: 300 kN loading capacity, 15 Hz maximum frequency, and 0.05 N load cell sensitivity. The fatigue tests are conducted at a frequency of 10 Hz. The fatigue testing machine and one of the torque arm test specimens used in the tests are shown in Figure 3.

The loading conditions for the fatigue tests are described below. As shown in Figure 3, the torque arm is fixed to the test frame at the left lower end. As a uniaxial testing machine is used, the test specimen is oriented at an angle of 28.8° to provide the multi-axial cyclic loads F_X and F_Y (see Figure 1). The resultant cyclic load applied at the upper right hole alternates between 1589.3 and -1141.4 N with a stress ratio of -0.718. The technical drawings of the right and the left grips are provided in Appendix 1. The grips are made of AISI 4140 steel.

Fatigue lives obtained after the testing of three different specimens are presented in Table 2. The average value of the fatigue life is 17,597 cycles, and the

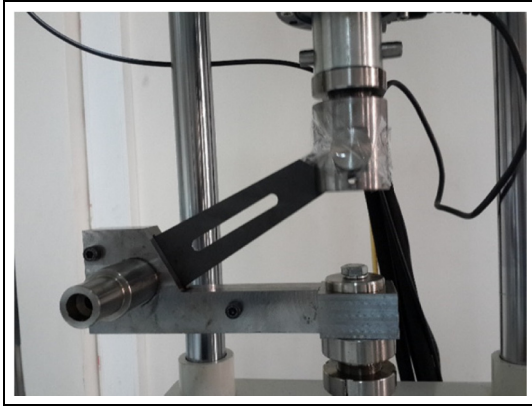


Figure 3. Fatigue testing machine and one torque arm test specimen.

Table 2. Fatigue testing machine and one torque arm test specimen.

Specimen	Number of cycles
S1	23,638
S2	12,508
S3	16,645
Average	17,597
Standard deviation	5626

standard deviation is 5625 cycles (32% of the average value). All specimens are observed to fail at the same location. To save space, only one of the specimens (specimen S1) is shown in Figure 4. In the tests conducted, crack is initiated on the surface at the contact interface between the torque arm and the grips.

Finite element modeling

In this section, the solid modeling of the torque arm is explained first. Then, the boundary conditions realized in the fatigue tests are discussed. Finally, determination of the proper mesh size and frictional contact modeling are discussed. Finite element modeling is performed using ANSYS Workbench 15 in a single-processor HP Z400 Workstation with Intel Xeon 2.67 GHz processor and 6.00 GB RAM.

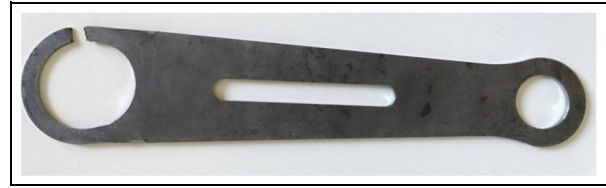


Figure 4. Specimen S1 after the fatigue test.

Solid modeling

To model the torque arm under fatigue test conditions, the solid models of the torque arm and the grips are generated first (see Figure 5). In the tests, the torque arm is placed in between the right and left grips. Instead of modeling the whole grips, only the parts of the grips that are satisfactory to model are modeled (see Figure 6). This procedure reduced the number of finite elements, thereby reducing the total analysis time. The final solid model is composed of nine different parts (see Figure 6); this ensures that smoother mesh can be generated in round sections and mesh density can be increased in critical sections.

Boundary conditions

Realistic modeling of the boundary conditions is important in structural analysis. A pictorial representation of the boundary conditions of the torque arm at fatigue testing conditions is shown in Figure 7. The torque arm is placed in the slot at the left grip; therefore, its displacements are constrained. The boundary condition BC1 constrains the displacements of the torque arm in all directions at the locations shown in Figure 7. The torque arm is constrained by a shaft passing through the left hole of the arm. The boundary condition BC2 allows the displacement of the center of the hole in the x -direction only while constraining the displacement in other directions. The boundary condition BC3 fixes the parts of the grip in all directions. The boundary condition BC4 models the friction between the torque arm and grip surfaces. The effect of the friction coefficient on the results is investigated later (see section "Finite element modeling at working conditions"). The last boundary condition includes the applied loads, which act as cyclic bearing loads.

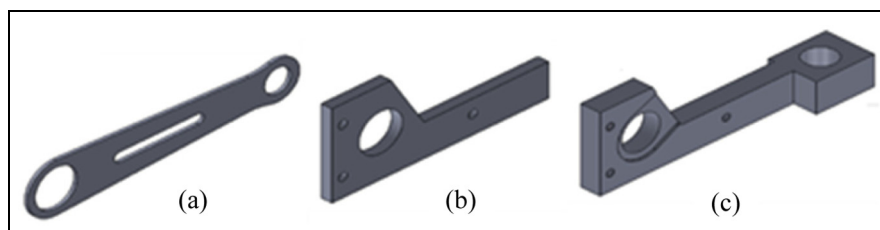


Figure 5. Solid models of (a) the torque arm, (b) the right grip, and (c) the left grip.

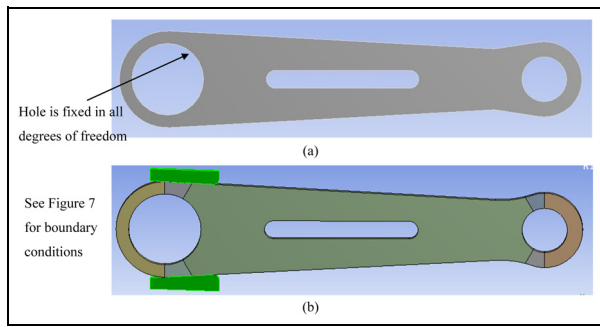


Figure 6. The final solid model used in fatigue analyses (a) for the actual working conditions and (b) test conditions.

Fatigue life estimation

The fatigue life of the torque arm is estimated by using the Smith–Watson–Topper relationship given in equation (2)

$$\sigma_{\max} \frac{\Delta \varepsilon}{2} = \frac{(\sigma'_f)^2}{E} (2N_f)^{2b} + \sigma'_f \varepsilon'_f (2N_f)^{b+c} \quad (2)$$

where σ_{\max} is the maximum stress of the given cycle, $\Delta \varepsilon$ is the total strain range, E is the modulus of elasticity, σ'_f is the fatigue strength coefficient, b is the fatigue strength exponent, ε'_f is the fatigue ductility coefficient, and c is the fatigue ductility exponent. A low-cycle fatigue criterion is used so that the effects of the elastic and plastic strain ranges are taken into account. The material properties are given in Table 1.

Meshing and frictional contact modeling

In this study, ANSYS Workbench Solid 185 elements (eight-noded hexahedral elements) are used in the finite element model. The global mesh density and the mesh density at the critical location are shown in Figure 8. The finite element mesh size and the friction coefficient used in the analysis have significant effects on the stress and fatigue life predictions. First, the variation of the maximum von Mises stress with the finite element mesh size and the friction coefficient is explored. Table 3

Table 3. Maximum von Mises stress (MPa) estimations for various element sizes and friction coefficient values corresponding to test conditions.

Friction coefficient	Element size				
	1 mm	0.75 mm	0.50 mm	0.40 mm	0.30 mm
No friction	1329.7	1215.0	1415.5	1677.0	1733.5
$\mu = 0.3$	526.0	536.0	521.4	494.1	484.2
$\mu = 0.5$	503.6	511.2	495.8	469.8	460.1
$\mu = 0.7$	1143.0	1045.0	1205.0	1421.5	1505.4

Table 4. Fatigue life estimations for various element sizes and friction coefficient values corresponding to test conditions.

Friction coefficient	Element size				
	1 mm	0.75 mm	0.50 mm	0.40 mm	0.30 mm
$\mu = 0.3$	16,745	15,504	17,361	21,868	23,788
$\mu = 0.5$	20,000	18,807	21,258	27,043	29,575

shows that using a frictionless contact or a large value of friction coefficient ($\mu = 0.7$) results in unrealistically large stress estimations. Therefore, the friction coefficient values of $\mu = 0.3$ and $\mu = 0.5$ are used. Fatigue life estimation for various element sizes and two different friction coefficient values are given in Table 4. It is found that the use of friction coefficient of $\mu = 0.3$ yields fatigue life predictions closer to the average fatigue life observed in the tests (17,597 cycles). It is also found that the use of 0.50 mm element size yields the best fatigue life prediction compared with the test results, along with corresponding CPU time as seen in Table 5.

Finite element modeling at working conditions

The actual working conditions of the torque arm are different from the fatigue test conditions due to our

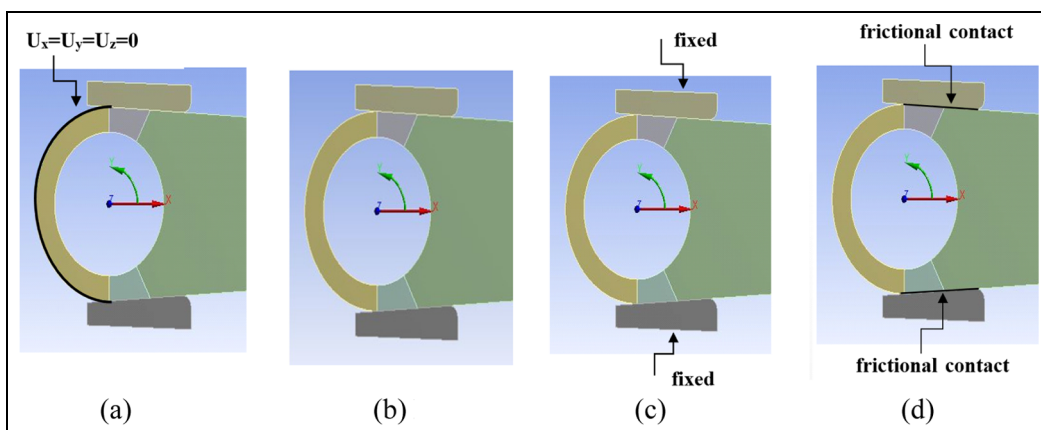


Figure 7. Pictorial representation of the boundary conditions corresponding to test conditions: (a) BC1, (b) BC2, (c) BC3, and (d) BC4.

Table 5. Approximate CPU times (in minutes) for various element sizes corresponding to test conditions.

Element size				
1 mm	0.75 mm	0.50 mm	0.40 mm	0.30 mm
5.5	13.9	67.9	174.6	272.7

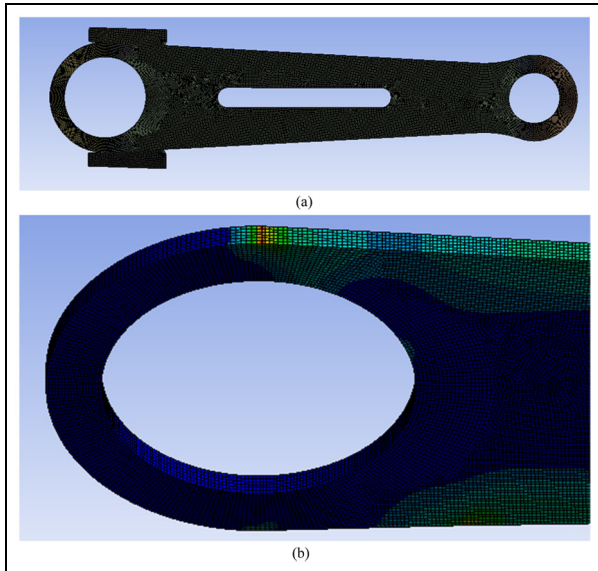


Figure 8. (a) Global mesh density and (b) mesh density at the critical location corresponding to test conditions.

inability to replicate the working conditions at the tests. At the working conditions, the torque arm is fixed to the chassis at the left end and the cyclic loads F_X and F_Y transferred from the rear wheels are applied at the right end. Therefore, the boundary conditions for the working conditions are relatively simple to model in the finite element study. The displacements in all directions are set to zero at the surface of the left hole, while the cyclic loads at the right hole are applied as bearing loads.

The maximum von Mises stress developed and the fatigue life of the initial design of the torque arm are computed as 319.1 MPa and 78,068 cycles, respectively. Therefore, the two constraint parameters appearing in equation (1) are set to $(\sigma_{VM})_{ini} = 319.1 \text{ MPa}$ and $(N_f)_{ini} = 78,068 \text{ cycles}$, respectively. The mass of the initial design is 0.1966 kg.

SSM

It is well known in surrogate modeling studies that as the size of the design space reduces, the accuracy of the surrogate model increases.⁴⁸ SSM is based on generating a small subregion in the design space, constructing surrogate model in this subregion, performing optimization in this subregion, using the optimum found as

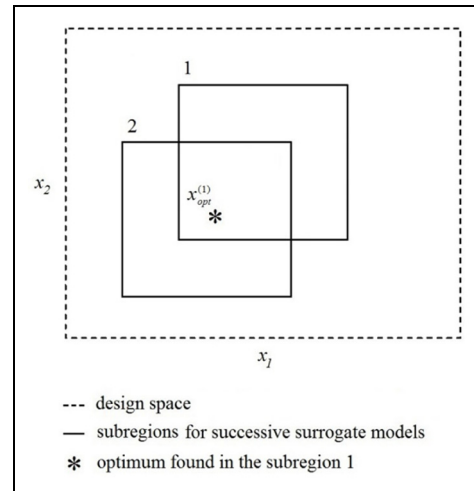


Figure 9. Successive surrogate modeling scheme.

the initial point for a successive subregion, and repeating this procedure until convergence. Figure 9 depicts the SSM scheme for the first two iterations. Subregion 1 is constructed around the initial design of the torque arm. A surrogate model is constructed within subregion 1, and the optimum in this subregion ($x_{opt}^{(1)}$) is obtained. The successive subregion (that is, subregion 2) is generated around $x_{opt}^{(1)}$, and the optimum in this new subregion ($x_{opt}^{(2)}$) is obtained. This procedure continues till convergence. In this study, the convergence criterion is reduction in the relative change of the objective function below 1% in subsequent steps. It is noted that the ANSYS Workbench Design Exploration toolbox is used to conduct optimization in each subregion.

Various heuristic schemes have been proposed to tune the size of the subregion.^{18,19} The rule of thumb is to reduce the size of the subregion if the surrogate model is not accurate enough. However, if the surrogate model is accurate enough, the size of the subregion is usually unchanged. In this study, we kept the size of the subregions small enough to guarantee an acceptable accuracy. Therefore, the lower and upper bounds of the design variables in each subregion are selected as 80% and 120% of the starting point (or the initial point) of the subregion.

Results

The optimization of the torque arm is performed using two different approaches. First, the global surrogate modeling approach is used. Quadratic response surface models are generated over the entire design space and optimization is performed. Second, the SSM approach is used. Again, quadratic response surface models are generated over each successive subregion. The reason for using global surrogate modeling approach in addition to successive response surface approach is to provide a baseline for comparison.

Table 6. Lower and upper bounds of the design variables and optimum values of the design variables.

Design variable	Initial value (mm)	Lower limit (mm)	Upper limit (mm)	Optimum obtained with 50 simulations (mm)	Optimum obtained with 100 simulations (mm)
d_1	5	3	10	10	10
d_2	5	3	10	4.7	4.5
h_1	60	40	80	40	40
h_2	135	108	162	113.6	115.5
v_1	10	7	18	18	18

Table 7. Performance of the optimum design obtained using global surrogate modeling corresponding to actual working conditions.

	50 samples			100 samples		
	Surrogate model prediction	FEA result	Error (%)	Surrogate model prediction	FEA result	Error (%)
Mass (kg)	0.1465	0.1464	0.1	0.1462	0.1460	0.1
Maximum von Mises stress (MPa)	319.1	277.3	15.1	318.0	278.0	14.3
Fatigue life (cycles)	90,271	162,150	44.3	78,069	160,540	51.4

FEA: finite element analysis.

Quadratic response surfaces are in the form of a second-degree algebraic polynomial function that can be expressed as

$$\hat{f}(\mathbf{x}) = b_0 + \sum_{i=1}^L b_i x_i + \sum_{i=1}^L b_{ii} x_i^2 + \sum_{i=1}^{L-1} \sum_{j=i+1}^L b_{ij} x_i x_j \tag{3}$$

where \hat{f} is the response surface approximation of the actual response function, f ; L is the number of variables in the input vector \mathbf{x} ; and b_0 , b_i , b_{ii} , and b_{ij} are the unknown coefficients to be determined by the least-squares technique.

Optimization results based on global surrogate modeling

In global surrogate modeling, the training points are generated over the entire design space. The number of training points is chosen as 10 times the number of design variables, following the suggestion of Jones et al.⁴⁹ The bounds of the design variables are determined based on earlier studies^{43,44} and are given in Table 6.

As we have five design variables, 50 training points are used in surrogate model generation and the optimization is performed. The optimum values of the design variables are given in the fifth column of Table 6. For the optimum design found, the surrogate model predictions are compared with the finite element results as shown in Table 7. It can be seen that surrogate model predictions are conservative, but inaccurate.

The number of training points is then increased from 50 to 100 in order to increase the accuracy of the surrogate models. The optimum values of the design

variables are given in the last column of Table 6. For the optimum design found, the surrogate model predictions are compared with the finite element analysis results as presented in Table 7. It is again noticed that surrogate model predictions are conservative, but inaccurate. Table 7 also shows that increasing the number of training points from 50 to 100 neither increases the accuracy of the surrogate model nor improves the optimization results significantly, so no further increase in the number of training points beyond 100 is pursued.

Table 7 shows that the optimization results based on global surrogate modeling correspond to a reduced mass of the torque arm, from 0.1966 to 0.1460 kg (25.7% reduction). The fatigue life and the maximum von Mises stress constraints are overly satisfied, indicating that the material distribution in the design domain is not optimal.

Optimization results based on SSM

In SSM, a smaller subregion is constructed in the design space and the training points are generated over this subregion. The lower and upper bounds of the design variables in the subregion are selected as 80% and 120% of the initial design of the torque arm. Fifty training points are generated in this subregion and quadratic response surface models are generated. Optimization is performed within this subregion using the constructed surrogate models. For the optimum design found, the surrogate model predictions are compared with the finite element analysis results, and it is found that the surrogate model predictions are quite accurate (see Table 8). The subsequent subregion is constructed around the optimum found in the previous step, 50 training points are generated in this subregion,

Table 8. Optimization results obtained using successive surrogate modeling corresponding to actual working conditions.

	Subregion 1	Subregion 2	Subregion 3	Subregion 4	Subregion 5
Lower and upper limits of the design variables					
d_1 (mm)	[4, 6]	[4, 8]	[6, 10]	[9, 11]	[11, 11]
d_2 (mm)	[4, 6]	[4, 6]	[5, 6]	[4.5, 5.5]	[4, 5.5]
h_1 (mm)	[48, 72]	[43, 57]	[41, 45]	[38, 44]	[38, 38]
h_2 (mm)	[122, 148]	[108, 132]	[110, 120]	[110, 120]	[115, 125]
v_1 (mm)	[8, 12]	[9, 15]	[13.5, 16.5]	[15, 18]	[18, 18]
Optimization results					
d_1 (mm)	6.0	8.0	10.0	11.0	11.0
d_2 (mm)	5.4	5.3	5.0	4.9	4.54
h_1 (mm)	49.6	43.0	41.0	38.0	38.0
h_2 (mm)	122.0	115.5	118.8	120.0	123.0
v_1 (mm)	12.0	15.0	16.5	18.0	18.0
Performance of optimum designs					
Predicted mass (kg)	0.1846	0.1658	0.1515	0.1404	0.1401
FEA mass (kg)	0.1836	0.1650	0.1515	0.1405	0.1401
Predicted maximum von Mises stress (MPa)	319.1	319.0	319.1	319.1	319.1
FEA maximum von Mises stress (MPa)	318.2	316.8	320.0	315.2	319.0
Predicted fatigue life (cycles)	78,068	81,180	82,320	80,280	78,074
FEA fatigue life (cycles)	79,228	80,988	77,088	83,081	78,194

FEA: finite element analysis.

Table 9. Comparison of optimization results (corresponding to actual working conditions) obtained using global surrogate modeling and successive surrogate modeling.

	Initial design	Global surrogate modeling optimum	Successive surrogate modeling optimum
Values of design variables			
d_1 (mm)	5	10.0	11.0
d_2 (mm)	5	4.54	4.54
h_1 (mm)	60	40.0	38.0
h_2 (mm)	135	115.5	123.0
v_1 (mm)	10	18.0	18.0
Performances of the designs evaluated through FEA			
Mass (kg)	0.1966	0.1460	0.1401
Maximum von Mises stress (MPa)	319.1	278.0	319.0
Fatigue life (cycles)	78,068	160,540	78,194

FEA: finite element analysis.

and optimization is performed within this subregion. This procedure is continued until the change of the objective function in the subsequent steps is reduced below 1%. Table 8 shows that the convergence is achieved in five iterations. Table 8 also shows that SSM-based optimization reduces the mass of the torque arm from 0.1966 to 0.1401 kg (28.7% reduction). The fatigue life and maximum von Mises stress values are very close to those of the initial design. Variations in the design variables, mass, maximum von Mises stress, and fatigue life through SSM are depicted in Figure 10.

Finally, the optimization results obtained through the global surrogate modeling approach are compared with the ones obtained with the SSM approach (see Table 9). The masses of the optimum designs obtained through global surrogate modeling and SSM are found

to be 0.1460 and 0.1401 kg, respectively. That is, the optimum design found through SSM is 4% lighter than the one found through global surrogate modeling. For the optimum design obtained through global surrogate modeling, the maximum von Mises stress developed in the torque arm is 278 MPa (12.9% smaller than that of the initial design), and the fatigue life of the torque arm is 160,540 cycles (105.6% larger than that of the initial design). As the fatigue life and stress constraints are overly satisfied, this means that the material distribution in the design domain is not optimal. For the optimum design obtained through SSM, on the contrary, the maximum von Mises stress developed in the torque arm is 319.0 MPa and the fatigue life of the torque arm is 78,194 cycles. These fatigue life and stress values are very close to those of the initial design. The distribution of the von Mises stress and fatigue life for the initial

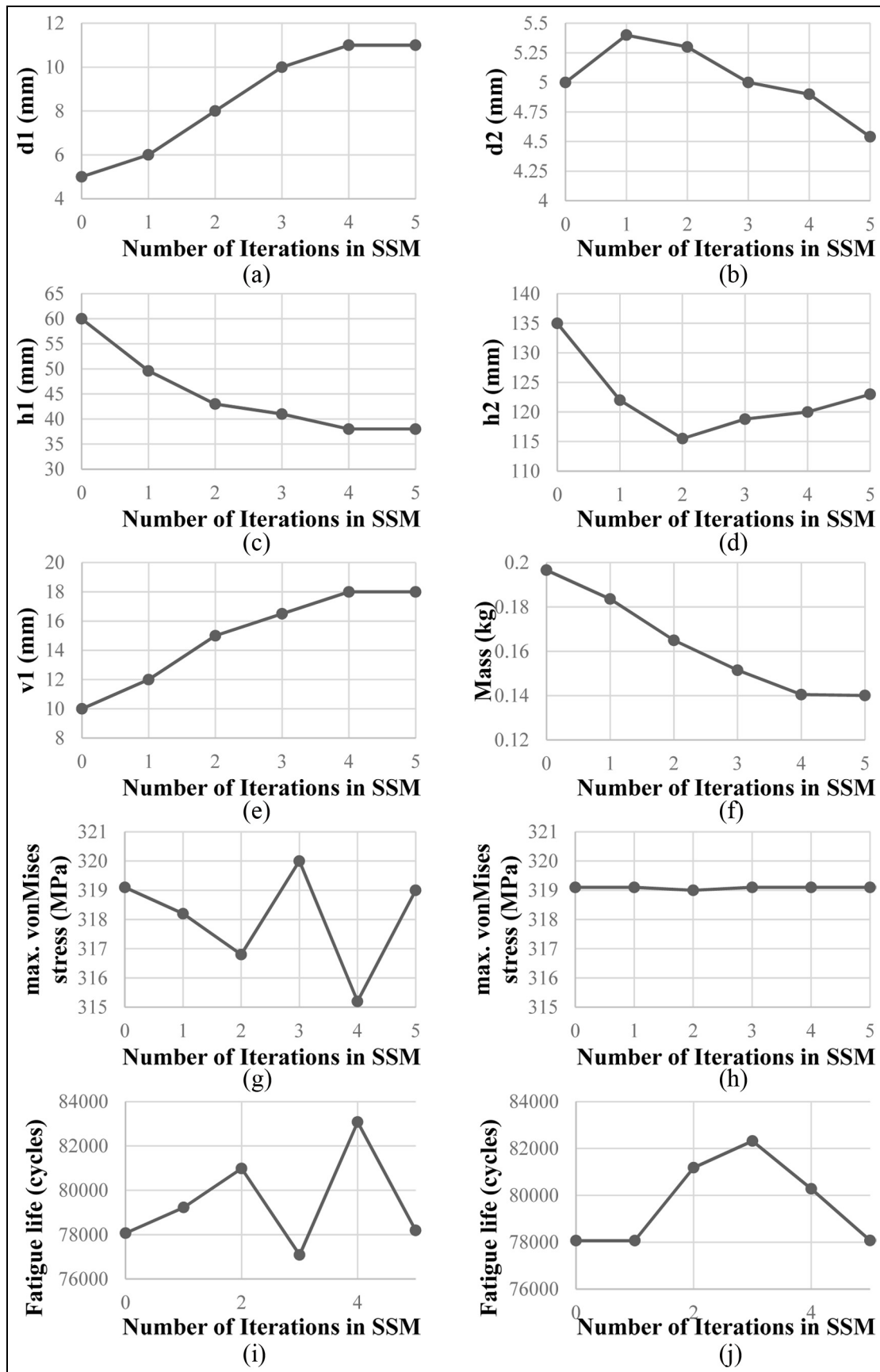


Figure 10. Variation of the (a–e) design variables, (f) mass, (g–h) maximum von Mises stress, and (i–j) fatigue life through successive surrogate modeling corresponding to actual working conditions: (a) design variable d_1 , (b) design variable d_2 , (c) design variable h_1 , (d) design variable h_2 , (e) design variable v_1 , (f) mass, (g) finite element analysis (FEA) maximum von Mises stress, (h) predicted maximum von Mises stress, (i) FEA fatigue life and (j) predicted fatigue life. SSM: successive surrogate modeling.

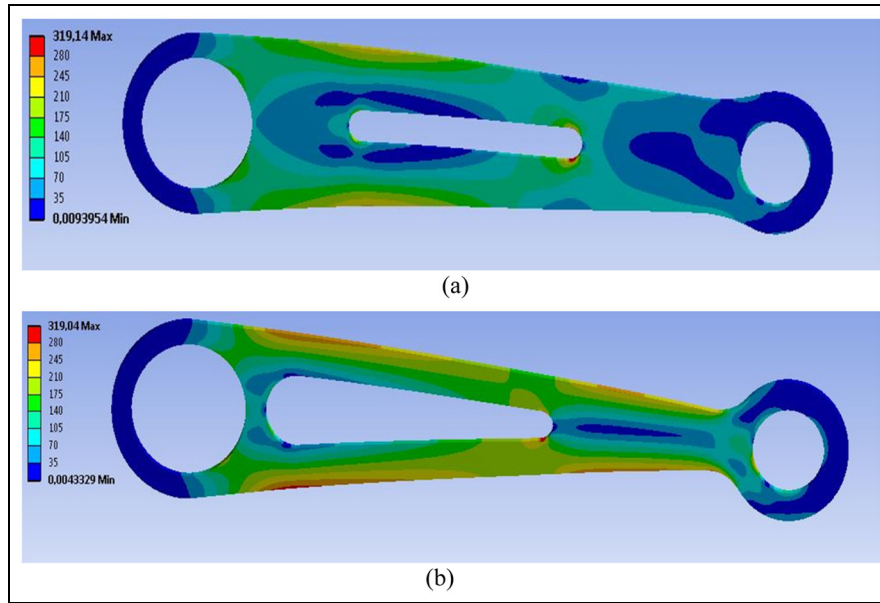


Figure 11. Distribution of von Mises stress (MPa) for (a) initial and (b) optimum designs (corresponding to actual working conditions).

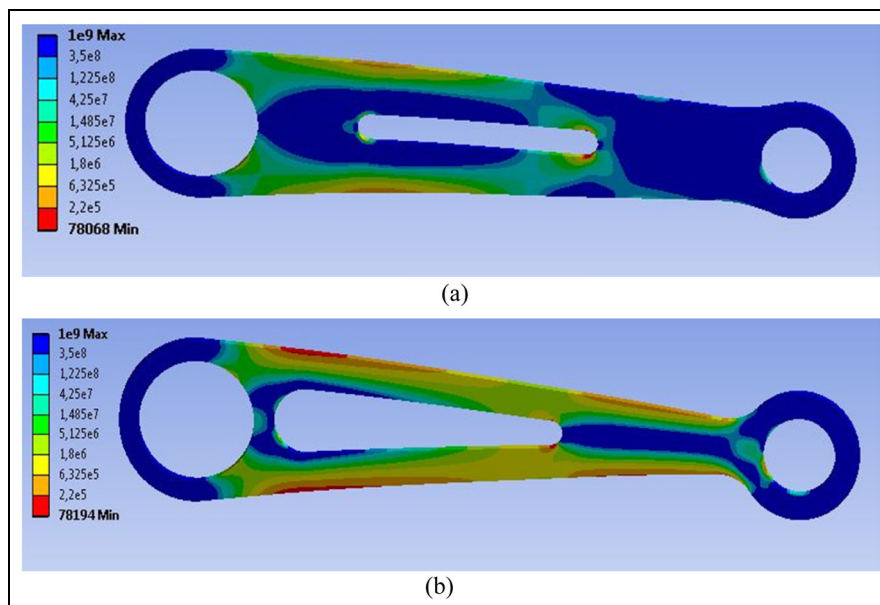


Figure 12. Distribution of fatigue life (cycles) for (a) initial and (b) optimum designs (corresponding to actual working conditions).

design and the optimum design is shown in Figures 11 and 12, respectively.

Concluding remarks

In this study, design optimization of an automobile torque arm subjected to cyclic loading was performed. Starting from an available initial design, the shape of the torque arm was optimized for minimum weight such that the fatigue life of the torque arm did not fall below that of the initial design and the maximum von

Mises stress developed in the torque arm did not exceed that of the initial design. Surrogate-based optimization approach was used to reduce the computational cost. Global surrogate modeling and SSM approaches were compared. From the results obtained, the following observations were made:

- In global surrogate modeling, when the number of training points was 10 times the number of variables (a widely used practice), the constructed surrogate models were not accurate enough. Increasing

the number of training points to 20 times the number of variables did not increase the accuracy and optimization results significantly.

- Global surrogate modeling-based optimization reduced the mass of the torque arm from 0.1966 to 0.1460 kg (25.7% reduction). The fatigue life and the maximum von Mises stress constraints were overly satisfied, indicating that the material distribution was not optimal.
- In SSM, when the number of training points was 10 times the number of variables, the constructed surrogate models were sufficiently accurate.
- SSM-based optimization reduced the mass of the torque arm from 0.1966 to 0.1401 kg (28.7% reduction). The fatigue life and the maximum von Mises stress values were very close to those of the initial design.
- The optimum design found through SSM is 4% lighter than the one found through global surrogate modeling.

Acknowledgements

The authors gratefully acknowledge the support provided by The Scientific and Technological Research Council of Turkey (TÜBİTAK), under award MAG-214M205.

Declaration of conflicting interests

The author(s) declared no potential conflicts of interest with respect to the research, authorship, and/or publication of this article.

Funding

The author(s) received no financial support for the research, authorship, and/or publication of this article.

References

1. Venkataraman S and Haftka RT. Structural optimization complexity: what has Moore's law done for us? *Struct Multidiscip O* 2004; 28: 375–387.
2. Fang H, Solanki K and Horstemeyer M. Numerical simulations of multiple vehicle crashes and multidisciplinary crashworthiness optimization. *Int J Crashworthines* 2005; 10: 161–172.
3. Box GEP and Draper N. *Response surfaces, mixtures, and ridge analyses*. 2nd ed. New York: Wiley, 2007.
4. Myers RH, Montgomery DC and Anderson-Cook CM. *Response surface methodology: process and product optimization using designed experiments*. 3rd ed. New York: Wiley, 2015.
5. Sacks J, Welch WJ, Mitchell TJ, et al. Design and analysis of computer experiments. *Stat Sci* 1989; 4: 409–435.
6. Martin JD and Simpson TW. Use of Kriging models to approximate deterministic computer models. *AIAA J* 2005; 43: 853–863.
7. Hardy RL. Multiquadric equations of topography and other irregular surfaces. *J Geophys Res* 1971; 76: 1905–1915.
8. Buhmann MD. *Radial basis functions: theory and implementations*. New York: Cambridge University Press, 2003.
9. Smith M. *Neural networks for statistical modeling*. New York: Van Nostrand Reinhold, 1993.
10. Bishop CM. *Neural networks for pattern recognition*. New York: Oxford University Press, 1995.
11. Gunn SR. Support vector machines for classification and regression. Technical report, Image Speech and Intelligent Systems Research Group, University of Southampton, Southampton, 1997.
12. Clarke SM, Griebisch JH and Simpson TW. Analysis of support vector regression for approximation of complex engineering analyses. *J Mech Des: T ASME* 2005; 127: 1077–1087.
13. Goel T, Haftka RT, Shyy W, et al. Ensemble of surrogates. *Struct Multidiscip O* 2007; 33: 199–216.
14. Acar E and Rais-Rohani M. Ensemble of metamodels with optimized weight factors. *Struct Multidiscip O* 2009; 37: 279–294.
15. Ferreira WG and Serpa AL. Ensemble of metamodels: the augmented least squares approach. *Struct Multidiscip O* 2016; 53: 1019–1046.
16. Queipo NV, Haftka RT, Shyy W, et al. Surrogate-based analysis and optimization. *Prog Aerosp Sci* 2005; 41: 1–28.
17. Wang GG and Shan S. Review of metamodeling techniques in support of engineering design optimization. *J Mech Des: T ASME* 2007; 129: 370–380.
18. Roux WJ, Stander N and Haftka RT. Response surface approximations for structural optimization. *Int J Numer Meth Eng* 1998; 42: 517–534.
19. Stander N and Craig KJ. On the robustness of a simple domain reduction scheme for simulation-based optimization. *Eng Computation* 2002; 19: 431–450.
20. Sobieszczanski-Sobieski J, Kodiyalam S and Yang RY. Optimization of car body under constraints of noise, vibration, and harshness (NVH), and crash. *Struct Multidiscip O* 2001; 22: 295–306.
21. Youn BD, Choi KK, Yang R-J, et al. Reliability-based design optimization for crashworthiness of vehicle side impact. *Struct Multidiscip O* 2004; 26: 272–283.
22. Zhang Y, Zhu P and Chen G. Lightweight design of automotive front side rail based on robust optimization. *Thin Wall Struct* 2007; 45: 670–676.
23. Lee K-H and Kang D-H. Structural optimization of an automotive door using the kriging interpolation method. *Proc IMechE, Part D: J Automobile Engineering* 2007; 221: 1525–1534.
24. Kim JK, Kim YJ, Yang WH, et al. Structural design of an outer tie rod for a passenger car. *Int J Automot Techn* 2011; 12: 375–381.
25. Liu Z, Lu J and Zhu P. Lightweight design of automotive composite bumper system using modified particle swarm optimizer. *Compos Struct* 2016; 140: 630–643.
26. Kiani M, Gandikota I, Parrish A, et al. Surrogate-based optimisation of automotive structures under multiple crash and vibration design criteria. *Int J Crashworthines* 2013; 18: 473–482.
27. Hu XJ, Yang B, Lei YL, et al. Automotive shape optimization using the radial basis function model based on a parametric surface grid. *Proc IMechE, Part D: J Automobile Engineering* 2016; 230: 1808–1821.
28. Yildiz BS, Lekesiz H and Yildiz AR. Structural design of vehicle components using gravitational search and

- charged system search algorithms. *Mater Test* 2016; 58: 79–81.
29. Karagöz S and Yildiz AR. A comparison of recent meta-heuristic algorithms for crashworthiness optimisation of vehicle thin-walled tubes considering sheet metal forming effects. *Int J Vehicle Des* 2017; 73: 179–188.
 30. Zhu P, Pan F, Chen W, et al. Use of support vector regression in structural optimization: application to vehicle crashworthiness design. *Math Comput Simulat* 2012; 86: 21–31.
 31. Fan KK, Chiu CH and Yang CC. Green technology automotive shape design based on neural networks and support vector regression. *Eng Computation* 2014; 31: 1732–1745.
 32. Song KS, Kang SO, Jun SO, et al. Aerodynamic design optimization of rear body shapes of a sedan for drag reduction. *Int J Automot Techn* 2012; 13: 905–914.
 33. Zhu WF, Wang J and Lin PJ. Numerical analysis and optimal design for new automotive door sealing with variable cross-section. *Finite Elem Anal Des* 2014; 91: 115–126.
 34. Kurtaran H, Eskandarian A, Marzougui D, et al. Crashworthiness design optimization using successive response surface approximations. *Comput Mech* 2002; 29: 409–421.
 35. Craig KJ, Stander N, Dooge DA, et al. Automotive crashworthiness design using response surface-based variable screening and optimization. *Eng Computation* 2005; 22: 38–61.
 36. Thiele M, Mullerschön H, van den Hove M, et al. Optimization of an adaptive restraint system using LS-OPT and visual exploration of the design space using D-SPEX. In: *Proceedings of the 9th international LS-DYNA users conference*, Detroit, MI, 4–6 June 2006.
 37. Liang CC and Le GN. Bus rollover crashworthiness under European standard: an optimal analysis of superstructure strength using successive response surface method. *Int J Crashworthines* 2009; 14: 623–639.
 38. Gustafsson E and Strömberg N. Shape optimization of castings by using successive response surface methodology. *Struct Multidiscip O* 2008; 35: 11–28.
 39. Zhang Y, Sun GY, Li GY, et al. Identification of material parameters for high strength steel under impact loading. *Adv Sci Lett* 2011; 4: 708–714.
 40. Pajunen S and Heinonen O. Automatic design of marine structures by using successive response surface method. *Struct Multidiscip O* 2014; 49: 863–871.
 41. Botkin ME. Shape optimization of plate and shell structures. *AIAA J* 1982; 20: 268–273.
 42. Wang X, Zhou J and Hu Y. A physics-based parameterization method for shape optimization. *Comput Method Appl Mech Eng* 1999; 175: 41–51.
 43. Kim NH, Choi KK and Botkin ME. Numerical method for shape optimization using meshfree method. *Struct Multidiscip O* 2003; 24: 418–429.
 44. Picheny V, Kim NH, Haftka RT, et al. Conservative predictions using surrogate modeling. In: *Proceedings of the 49th AIAA/ASME/ASCE/AHS/ASC structures, structural dynamics, and materials*, Schaumburg, IL, 7–10 April 2008.
 45. Karenĭ, Yildiz AR, Kaya N, et al. Hybrid approach for genetic algorithm and Taguchi's method based design optimization in the automotive industry. *Int J Prod Res* 2006; 44: 4897–4914.
 46. Yildiz BS and Lekesiz H. Fatigue-based structural optimisation of vehicle components. *Int J Vehicle Des* 2017; 73: 54–62.
 47. Schütz D, Klätschke H and Heuler P. *Standardized multi-axial load sequences for car wheel suspension components—car loading standard—CARLOS multi*. Report no. FB-201, 1994. Darmstadt: Fraunhofer-Institut für Betriebsfestigkeit LBF.
 48. Forrester AIJ and Keane AJ. Recent advances in surrogate-based optimization. *Prog Aerosp Sci* 2009; 45: 50–79.
 49. Jones D, Schonlau M and Welch W. Efficient global optimization of expensive black-box functions. *J Global Optim* 1998; 13: 455–492.

Appendix I

Technical drawings of the right and the left grips

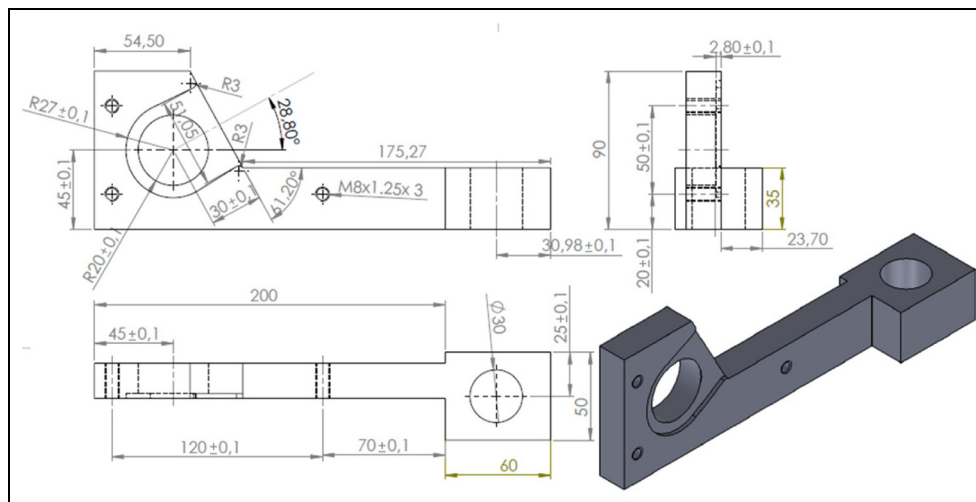


Figure I3. Technical drawing of the left grip (dimensions in mm).

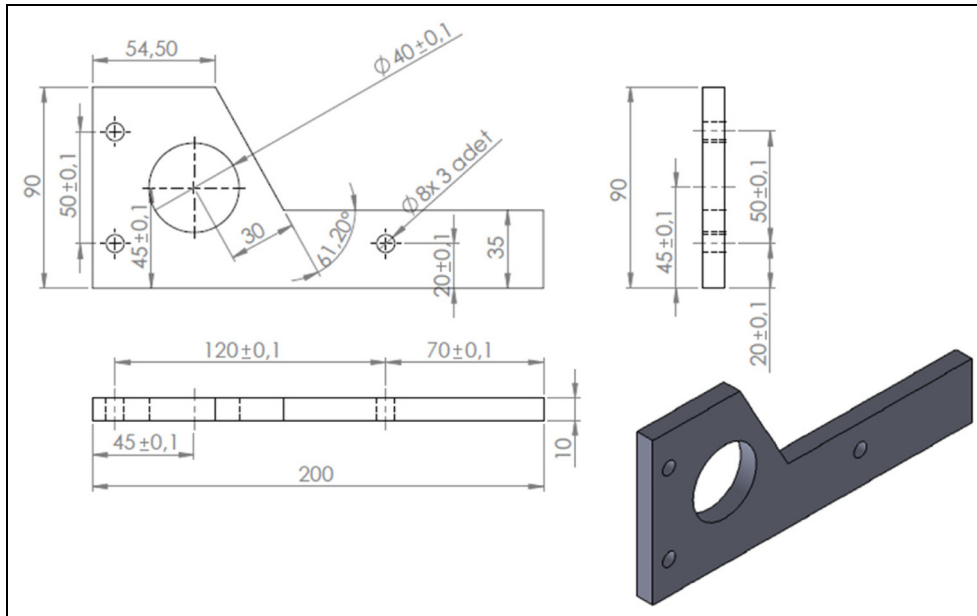


Figure 14. Technical drawing of the right grip (dimensions in mm).